Wavelet-based Model Predictive Control of PWR Nuclear Reactor using Multi-Scale Subspace Identification

Vineet Vajpayee[1], Victor Becerra[1], Nils Bausch[1], and Jiamei Deng[2]

[1] School of Energy and Electronic Engineering, University of Portsmouth, Portsmouth, PO1 3DJ, United Kingdom.
vineet.vajpayee@port.ac.uk, victor.becerra@port.ac.uk, nils.bausch@port.ac.uk

[2] School of Computing, Creative Technologies & Engineering, Leeds Beckett University, Leeds, LS6 3QR, United Kingdom.
j.deng@leedsbeckett.ac.uk

Abstract. This work presents multi-scale model predictive control design scheme employing wavelet basis function. The proposed scheme is established upon multi-scale subspace identification technique. It is aimed to utilize the proficiency of wavelets in multi-scale data projection and the robustness of subspace identification during estimation in a model predictive control set-up. The multi-scale state-space models estimated at different scales are used for output prediction and for designing predictive control strategy. The competence of the proposed approach is established for constrained load-following problem of a pressurized water-type nuclear reactor. In addition, the fault-tolerant capability of the control algorithm is also tested.

Keywords: MPC, Multi-resolution, Nuclear reactor, PWR, Subspace Identification, Wavelet

1 Introduction

In the current scenario, model predictive control (MPC) is seen to be as a prevalent advanced modern control design strategies in the process industries [1]. Its wide applicability is because of its capability to handle process constraints with an ease in adaptability to ever changing operating settings in a plant [2]. MPC solves an optimization problem at each sampling instant to regulate future control input actions over a time horizon. In the receding horizon-based MPC strategy, only the first control move in the series is fed to the process and the same strategy is reiterated at the succeeding time instant [3]. Primarily, MPC requires a suitable mathematical model of the underlying process for designing controller. In case of complex multi-scale processes such as nuclear reactor, it is imperative that an appropriately defined model is used to attain good dynamic response. A nuclear reactor consists of simultaneously evolving slow and fast modes exhibiting behaviour in multiple time-scales. Traditionally,

it is modelled at single-scale using first principles approach. However, such a system representation is not preferable for control purposes particularly in refurbishing control design technique in an existing nuclear plant which has aged over time. It has been reported in literature that modelling of multi-scale systems by single-scale approaches may degrade system response and sometimes it may cause ill-conditioning. Thus, the adopted modelling and control design approach should consider the existence of time-scales to avoid performance deterioration.

Over the years, different modeling approaches exploiting two and three time-scales property of nuclear reactor system have been proposed [4]. However, different multi-scale aspects in a process are unclear in measurement space. Thus, it is crucial to have process visualization in a multi-resolution set-up. Wavelets are the new families of generalized basis functions for the better representation of signals simultaneously in time and scale. The modelling problem is often simplified by reformulating in multi-resolution using wavelet basis functions. The objective translates to building linear descriptions at different resolution of a non-linear system. Model identification employing wavelet basis is effective owing to its exceptional approximation capability in multi-resolution. Wavelet basis function efficiently extracts local available knowledge from the data in time-scale plane. Therefore, the wavelet identified model is capable of capturing complexities such as non-linearity, integrating, and multiple time-scale behaviour effectively in fewer parameters.

The integration of wavelets and wavelet-like basis with MPC is suggested by Elias-Juarez and Kantor [5]. An approach for improving computational efficiency of MPC for systems with multiple time-scales using wavelet basis is proposed in [6]. Feng *et al.* [7] developed a technique for simultaneous MPC and identification involving time-scale system modelling. The notion of multi-scale system modelling on dyadic trees formulated by Basseville *et al.* [8] has been employed in literature for developing multi-scale MPC techniques. For instance, a multi-scale MPC strategy on the dyadic trees is developed by Stephanopoulos *et al.* [9, 10]. Zhang and Bentsman [11] suggested wavelet approximation-based MPC approach for a non-linear system. A MPC scheme using the notion of consistency in wavelet projections is proposed in [12]. Recently, a nonlinear MPC using wavelet series of differentially flat systems has been developed [13]. However, a different stance has been adopted in this proposed work. Here, black-box state-space models are identified directly from measurements at different scales and are used for output prediction and then employed in designing control law. Hence, enhancing the modelling in multi-resolution results into effective control of modes in multiple time-scales.

The primary objective of the proposed work is to formulate a predictive control strategy using wavelet-based state-space identified model. A non-linear process is estimated by a set of linear models operating at distinct time-scale. The identified models are employed to predict the output behaviour only at those scales where the process is evolving. The output predictions at significant scales are then fused using inverse wavelet operator. These fused or synthesized predictions are then used for optimization to find future control input. The

efficacy of the technique is validated in the load-following mode of operation of a pressurized water-type reactor (PWR).

The rest of the paper is organized as follows: Section 2 presents a brief introduction to multi-scale subspace identification. Section 3 proposed model predictive control strategy in multi-resolution. Application of proposed technique to PWR is given in Section 4. Finally, conclusions are drawn in Section 5 indicating main contributions.

2 Multi-scale Subspace Identification

Multi-scale subspace identification (MSID) is a projection space or time-scale domain based modelling technique for the estimation of system states directly from the wavelet projection of measurements. It establishes a definite correspondence in time-scale domain with the evolution of low order state-space sub-band models at different resolutions thereby spanning complete frequency band of the underlying process. MSID can be divided into two stages wherein the first stage is to represent the data in multi-resolution and the next stage is to identify models from the wavelet projections.

2.1 Multi-scale Data Representation

Wavelet transform is one of the established mechanism for representing measurements in multi-resolution. Wavelets are known as approximate Eigenfunctions of the convolution operator. They decouple system modes with sharp decay in correlation structure in projection space. Transforming the measurements to multi-resolution facilitates monitoring of various modes present in the data-set at different scales. The wavelet transform in multi-scale subspace identification can be implemented by integer discretization scheme as shown in Fig. 1 which demonstrates two level of wavelet decomposition. The measurements are recorded at scale $j = 0$ and they are known up to time instant k. A window of $2J$ observations is composed and decomposed into detail spaces at $j = 1, 2, \ldots, J$ and an approximation space at $j = J+1$. The wavelet decomposition is then performed on the one time step ahead translated window at instant $k + 1$ window. The similar procedure is iterated thereafter.

Consider recorded input (U) and output (Y) time-series data. The wavelet transformation is then given by

$$\begin{aligned} U^w &= \begin{bmatrix} U_{J+1}^T & U_J^T & U_{J-1}^T & \cdots & U_1^T \end{bmatrix}^T = WU; \\ Y^w &= \begin{bmatrix} Y_{J+1}^T & Y_J^T & Y_{J-1}^T & \cdots & Y_1^T \end{bmatrix}^T = WY; \end{aligned} \tag{1}$$

where U^w and Y^w are called as wavelet coefficients and comprised of approximation and details. The wavelet operator W is given by

$$\begin{aligned} W &= \left[\prod_{j=1}^{J} H_j^T \quad G_J^T \prod_{j=1}^{J-1} H_j^T \quad G_{J-1}^T \prod_{j=1}^{J-2} H_j^T \quad \cdots G_1^T \right]^T, \\ &= \begin{bmatrix} \tilde{H}_J^T & \tilde{G}_J^T & \tilde{G}_{J-1}^T \cdots & \tilde{G}_1^T \end{bmatrix}^T, \end{aligned} \tag{2}$$

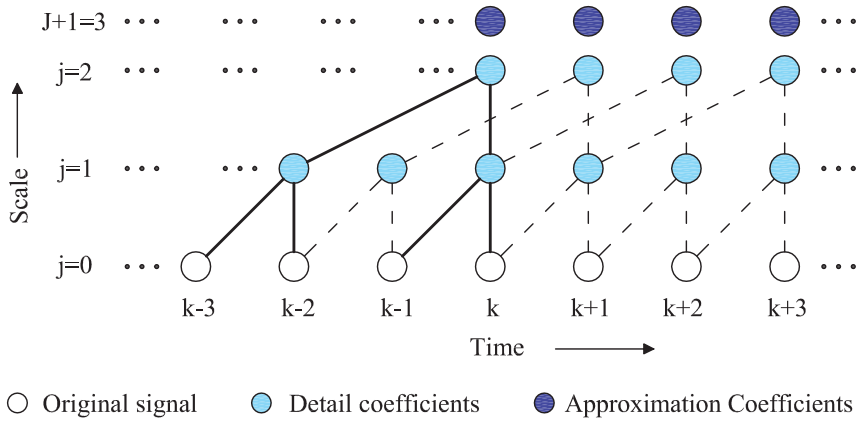

Fig. 1. Implementation of wavelet transform.

where $\tilde{H}_J\left(1 \times 2^J\right)$ and $\tilde{G}_J\left(2^{J-j} \times 2^J\right)$ are matrices of wavelet filter coefficients [14]. For Haar wavelet and $J = 2$, W is given by

$$W = \begin{bmatrix} \tilde{H}_2 \\ \tilde{G}_2 \\ \tilde{G}_1 \end{bmatrix} = \frac{1}{2} \begin{bmatrix} 1 & 1 & 1 & 1 \\ 1 & 1 & -1 & -1 \\ \sqrt{2} & -\sqrt{2} & 0 & 0 \\ 0 & 0 & \sqrt{2} & -\sqrt{2} \end{bmatrix}. \tag{3}$$

Measurements can be reconstructed back from wavelet coefficients by applying inverse wavelet transform ($\overline{W}$) as

$$\hat{U} = \overline{W} U^w; \quad \hat{Y} = \overline{W} Y^w, \tag{4}$$

where $\hat{U}$ and $\hat{Y}$ are reconstructed input and output respectively. For orthogonal wavelet transform, $\overline{W} = W^{-1} = W^T$.

An efficacious implementation of wavelet-based technique demands meticulous selection of wavelet and scale. The technique proposed here is built on Haar wavelet due to its aptness in closely locating features in time domain. Due to compact support it does not insert delay and calculates the transformation employing measurements from the present and past only. Scale or maximum depth of decomposition (J) is selected such that a minimum amount of data sets should strike the support of each basis and may be calculated from Fourier transform such that the magnitude of Fourier transform is above the noise floor-level [15], *i.e.*

$$\left|U\left(\pi/2^J\right)\right| \geq \left|U\left(\pi/f\right)\right|, \quad \left|Y\left(\pi/2^J\right)\right| \geq \left|Y\left(\pi/f\right)\right|. \tag{5}$$

Usually, all of the scales do not contribute in the process and for a parsimonious model description, computation of significant scales is critical. The prediction ability of estimated models may be utilized to compute significant scales [16].

2.2 Subspace Identification at Significant Scales

Consider a linear time invariant (LTI) system in *innovation* form at j^{th} scale, given by

$$\begin{aligned} x_j[k+1] &= A_j\, x_j[k] + B_j\, u_j[k] + K_j\, e_j[k], \\ y_j[k] &= C_j\, x_j[k] + D_j\, u_j[k] + e_j[k], \end{aligned} \tag{6}$$

where state $x_j[k] \in \mathbb{R}^{n_j}$, input $u_j[k] \in \mathbb{R}^{m_j}$, output $y_j[k] \in \mathbb{R}^{l_j}$, innovation $e_j[k] \in \mathbb{R}^{l_j}$, and error covariance matrix $E(e_j[k]e_j^T[k]) = S_j$. $A_j \in \mathbb{R}^{n_j \times n_j}$, $B_j \in \mathbb{R}^{n_j \times m_j}$, $K_j \in \mathbb{R}^{n_j \times l_j}$, $C_j \in \mathbb{R}^{l_j \times n_j}$, and $D_j \in \mathbb{R}^{l_j \times m_j}$ are respective system matrices at j^{th} scale. Let, the measurements are recorded for $k \in \{1, 2, \ldots, N\}$ and have been transformed into wavelet domain. Define, $U_{p,j} \in \mathbb{R}^{im_j \times (N-2i+1)}$ and $U_{f,j} \in \mathbb{R}^{im_j \times (N-2i+1)}$ as *past* and *future* Hankel matrices formed using input wavelet coefficients at j^{th} scale respectively as

$$\begin{aligned} U_{p,j} &= \begin{bmatrix} u_j[1] & u_j[2] & \cdots & u_j[N-2i+1] \\ u_j[2] & u_j[3] & \cdots & u_j[N-2i+2] \\ \vdots & \vdots & \ddots & \vdots \\ u_j[i] & u_j[i+1] & \cdots & u_j[N-i] \end{bmatrix} \\ U_{f,j} &= \begin{bmatrix} u_j[i+1] & u_j[i+2] & \cdots & u_j[N-i+1] \\ u_j[i+2] & u_j[i+3] & \cdots & u_j[N-i+2] \\ \vdots & \vdots & \ddots & \vdots \\ u_j[2i] & u_j[2i+1] & \cdots & u_j[N] \end{bmatrix}. \end{aligned} \tag{7}$$

Similarly, other Hankel matrices, $Y_{p,j} \in \mathbb{R}^{il_j \times (N-2i+1)}$, $Y_{f,j} \in \mathbb{R}^{il_j \times (N-2i+1)}$, $E_{p,j} \in \mathbb{R}^{il_j \times (N-2i+1)}$, and $E_{f,j} \in \mathbb{R}^{il_j \times (N-2i+1)}$ can be defined. Also, let $X_{p,j} \in \mathbb{R}^{n_j \times (N-2i+1)}$ and $X_{f,j} \in \mathbb{R}^{n_j \times (N-2i+1)}$ as

$$\begin{aligned} X_{p,j} &= \begin{bmatrix} x_j[1] & x_j[2] & \cdots & x_j[N-2i+1] \end{bmatrix}, \\ X_{f,j} &= \begin{bmatrix} x_j[i+1] & x_j[i+2] & \cdots & x_j[N-i+1] \end{bmatrix}. \end{aligned} \tag{8}$$

Multi-scale subspace identification estimates extended observability matrix from the recorded data at different scales. Thus, from (6)–(8), it follows that

$$\begin{aligned} Y_{f,j} &= \Gamma_{i,j} X_{f,j} + L_{u,j} U_{f,j} + L_{e,j} E_{f,j}, \\ &= L_{x,j} W_{p,j} + L_{u,j} U_{f,j} + L_{e,j} E_{f,j}, \end{aligned} \tag{9}$$

where $\Gamma_{i,j} \in \mathbb{R}^{il_j \times n_j}$ is the extended observability matrix. $L_{u,j} \in \mathbb{R}^{il_j \times im_j}$ and $L_{e,j} \in \mathbb{R}^{il_j \times il_j}$ are the deterministic and stochastic Toeplitz matrices. $L_{x,j}$ is the product of controllability and observability matrix. From (9), we can write,

$$\begin{bmatrix} L_{x,j} & L_{u,j} \end{bmatrix} = Y_{f,j} \begin{bmatrix} W_{p,j} \\ U_{f,j} \end{bmatrix}^{\dagger}, \tag{10}$$

where $W_{p,j} = \begin{bmatrix} Y_{p,j}^T & U_{p,j}^T \end{bmatrix}^T$ and $[.]^{\dagger}$ represents the Moore-Penrose pseudo-inverse. $L_{x,j}$ can be estimated using QR decomposition. The SVD can be utilized on the

weighted $L_{x,j}$ matrix to calculate observability matrix and thereafter A_j and C_j matrices as

$$\begin{aligned}\hat{A}_j &= \hat{\Gamma}^{\dagger}_{i-1,j}\left(\left[0_{(i-1)l_j\times l_j} \;\; I_{(i-1)l_j\times(i-1)l_j}\right]\times\hat{\Gamma}_{i,j}\right),\\ \hat{C}_j &= \left[I_{l_j\times l_j} \;\; 0_{l_j\times(i-1)l_j}\right]\times\hat{\Gamma}_{i,j}.\end{aligned} \tag{11}$$

$L_{e,j}$ can be estimated by projecting (9) onto a basis orthogonal to $\left[W^T_{p,j} \;\; U^T_{f,j}\right]^T$. Now, assume $\bar{e}_j[k] = F_j^{-1}e_j[k]$ with identity covariance matrix, we can extract K_j as [17],

$$\begin{bmatrix}\hat{F}_j\\ \hat{K}_j\hat{F}_j\end{bmatrix} = \begin{bmatrix}I_{l_j\times l_j} & 0_{l_j\times n_j}\\ 0_{(i-1)l_j\times l_j} & \hat{\Gamma}_{i-1,j}\end{bmatrix}^{-1} L_{e,j}\begin{bmatrix}F_j\\ 0_{(i-1)l_j\times l_j}\end{bmatrix}. \tag{12}$$

where $0_{l_j\times n_j}$ and $I_{l_j\times l_j}$ represent zero and identity matrices respectively. The remaining matrices can be computed as the least squares estimate of the predictor defined by

$$\bar{y}_j[k] = G_jB_{K,j}u_j\,[k] + \bar{D}_ju_j\,[k] + G_jx_{0,j} + \bar{e}_j[k], \tag{13}$$

where,

$$\begin{aligned}\bar{y}_j[k] &= \hat{F}_j^{-1}\left(I_j - \hat{C}_j\left(qI_j - \hat{A}_{K,j}\right)^{-1}\hat{K}_j\right)y_j[k],\\ \hat{A}_{K,j} &= \left(\hat{A}_j - \hat{K}_jC_j\right),\; B_{K,j} = B_j - \hat{K}_jD_j,\\ G_j &= \hat{F}_j^{-1}\hat{C}_j\left(qI_j - \hat{A}_{K,j}\right)^{-1},\; \bar{D}_j = \hat{F}_j^{-1}D_j.\end{aligned} \tag{14}$$

3 Model Predictive Control With Multiple Resolutions

MPC in multi-resolution set-up combines multi-scale subspace identification with the predictive controller. In MPC, a set of future controller actions are defined by optimizing a quadratic cost function. In the philosophy of receding horizon-based MPC, only the first of the control action is executed as the present control action. At the next sampling instant, the optimization is solved again and the similar procedure is then reiterated.

3.1 Problem Formulation

MPC problem can be defined as follows:
Given a future set-point
$\mathbf{r_f} = \left[r^T\,[t+1] \;\; r^T\,[t+2]\cdots r^T\,[t+N_p]\right]^T$,
and a prediction of output
$\hat{\mathbf{y}}_\mathbf{f} = \left[\hat{y}^T\,[t+1] \;\; \hat{y}^T\,[t+2]\cdots \hat{y}^T\,[t+N_p]\right]^T$,
find a control input sequence
$\mathbf{u_f} = \left[u^T\,[t+1] \;\; u^T\,[t+2]\cdots u^T\,[t+N_c]\right]^T$
such that the following cost function is optimized:

$$\left(\hat{\mathbf{y}}_\mathbf{f} - \mathbf{r_f}\right)^T Q_f\left(\hat{\mathbf{y}}_\mathbf{f} - \mathbf{r_f}\right) + \Delta\mathbf{u_f}^T R_f\Delta\mathbf{u_f}, \tag{15}$$

subjected to

$$\begin{array}{ll} U_{\min} \leq \mathbf{u_f} \leq U_{\max}; & \Delta U_{\min} \leq \Delta \mathbf{u_f} \leq \Delta U_{\max}; \\ Y_{\min} \leq \mathbf{y_f} \leq Y_{\max}; & \Delta Y_{\min} \leq \Delta \mathbf{y_f} \leq \Delta Y_{\max}. \end{array} \tag{16}$$

where,
$U_{\min} = \left[u_{\min}^T \cdots u_{\min}^T \right]^T$, $\Delta U_{\min} = \left[\Delta u_{\min}^T \cdots \Delta u_{\min}^T \right]^T$,
$Y_{\min} = \left[y_{\min}^T \cdots y_{\min}^T \right]^T$, $\Delta Y_{\min} = \left[\Delta y_{\min}^T \cdots \Delta y_{\min}^T \right]^T$,
and the same notation holds with subscript max terms. N_p and N_c are prediction and control horizons, with $N_c \leq N_p$. R_f and Q_f are positive definite and positive semi-definite weighing diagonal matrices penalizing rate of change of input and error between output and set-point respectively.

3.2 Prediction at Significant Scale

MPC depends up on the mathematical description of the process as a part of an optimization strategy. It computes future behaviour of the control input to determine the desired process performance. In the proposed scheme, the output predictions are first calculated from the multi-scale state-space identified model as a function of past values of inputs and outputs and of future control signals. The principle behind the advocated scheme is that the MPC banks upon a model of the process can use multi-scale model description to determine control actions at scales at which they manifest themselves. The estimated models are working at different time-scales thereby able to capture different phenomena occurring in the underlying process suitably. Thus, the resulting control action that is implemented at measurement space will contain contributions from other scales thereby enhancing performance. The block diagram depiction of the suggested MPC scheme is shown in Fig. 2. The inputs to and outputs from the multi-scale model are real-valued variables in measurement domain. The analysis half transforms the measurements at multiple resolutions using the wavelet. The significant scales are calculated for parsimonious model identification. The identified models are then employed in predicting outputs at respective scales. The central idea is to have predictions in the multi-resolution around significant scales using state-space identified models. The predictions are then combined by projecting wavelet prediction coefficients into measurement space using inverse wavelet operator. The synthesized predictions are then used in optimizer to design the future control input. The wavelet-based model has been proved to be of good capability. Furthermore, it has been found that the multi-scale state-space identified model performs better prediction of output in contrast to other classical single-scale identified models in terms of least-squares sense [18].

4 Application to Pressurized Water Reactor

4.1 Mathematical Model of PWR

For system identification and control purposes, the mathematical model of PWR can be suitably illustrated by point kinetics equation coupled with thermal hy-

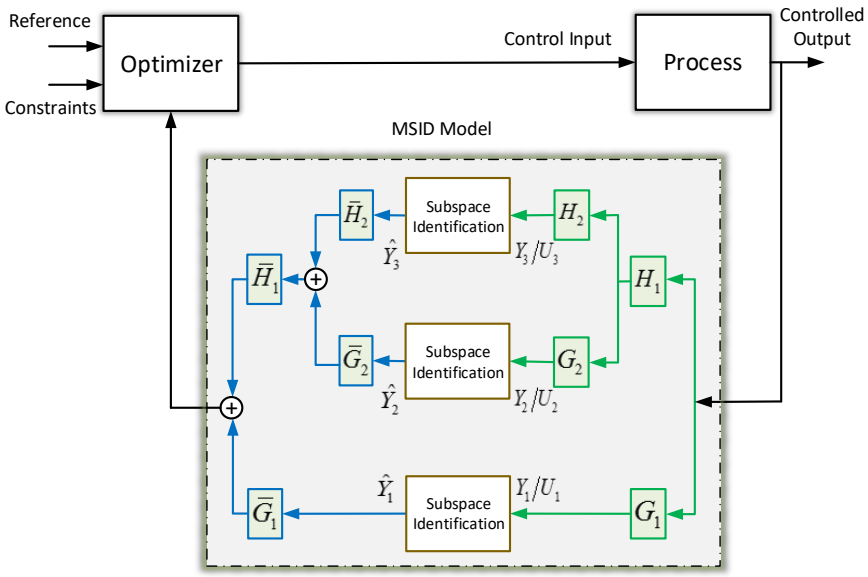

Fig. 2. Block diagram of the proposed control scheme for a decomposition depth of two.

draulics model considering six groups of delayed neutrons precursors' concentration. Here, the developed model is based on the following assumptions. The primary and secondary loops are modeled in which the primary loop is characterized by a nonlinear lumped model along with constant mass flow rate and pressure. The heat generated in the core is transferred by single-phase coolant only. The reactivity and power are considered as reactor system's input and output respectively [19].

$$\frac{dP}{dt} = \frac{\rho_T - \sum_{i=1}^{6} \beta_i}{\Lambda} P + \frac{\sum_{i=1}^{6} \beta_i C_i}{\Lambda}, \tag{17}$$

$$\frac{dC_i}{dt} = \lambda_i \left(P - C_i\right), \qquad i = 1, 2, \ldots, 6, \tag{18}$$

$$\frac{dT_f}{dt} = H_f P - \gamma_f \left(T_f - T_c\right), \tag{19}$$

$$\frac{dT_c}{dt} = -H_c \left(T_{out} - T_{in}\right) + \gamma_c \left(T_f - T_c\right), \tag{20}$$

$$\frac{dT_{in}}{dt} = \frac{1}{\tau_{cold}} \left(T_{cold} - T_{in}\right), \tag{21}$$

$$\frac{dT_{hot}}{dt} = \frac{1}{\tau_{hot}} \left(T_{out} - T_{hot}\right), \tag{22}$$

$$\frac{dT_{sg}}{dt} = -\frac{1}{\tau_{sg}}\left(T_{sg} - T_{hot}\right) - D_1 L_T, \tag{23}$$

$$T_{cold} = D_2 T_{sg} - D_3 T_{hot}, \tag{24}$$

$$\rho_T = \rho_{RR} + \alpha_f T_f + \alpha_c T_c. \tag{25}$$

where P is normalized neutronic power; λ_i, β_i, and C_i indicate decay constant, fraction of delayed neutrons, and normalized delayed neutron precursors' concentration of i^{th} group respectively; Λ represents prompt neutron life time; ρ_{RR} and ρ_T respectively denote reactivity contributed by regulating rod (RR) movement and the total reactivity; α_c and α_f are temperature coefficients of reactivity of coolant and fuel respectively; T_f is fuel temperature; T_{out} and T_{in} are core-outlet and inlet temperatures respectively; $T_c = \left(T_{out} + T_{in}\right)/2$ denotes average coolant temperature; H_f and H_c define the rate of rise of fuel and coolant temperatures respectively; γ_f and γ_c indicate the inverse of mean time for heat transfer from fuel to coolant and from core-outlet to inlet respectively; T_{cold}, T_{hot}, and T_{sg} respectively symbolize cold leg, hot leg and steam generator temperatures and are related to their respective time constants τ_{cold}, τ_{hot}, and τ_{sg}; D_1, D_2, and D_3 are constants; L_T is turbine load. Values of constants used in (17)–(25) are taken from [19, 20] and listed in Table 1.

4.2 Model Estimation

Initially, the nuclear reactor is considered to be operating at 50% full power. The model defined by (17)–(25) is then perturbed by the movement of RR. Fig. 3 and Fig. 4 respectively depict variation in reactivity due to the movement of RR and the corresponding reactor power output superimposed with 40 dB additive white Gaussian noise. The reactivity and power form the estimation data set for system identification exercise.

The Fourier transform of estimation data set is computed for finding the decomposition depth. The Fourier transform of measurements is shown in Fig. 5. It can be seen that the magnitude of the Fourier transform reaches the noise floor level roughly afterwards $\pi/124$ rad/sample. Thus, the maximum scale for decomposition is selected such that $\pi/2^J \geq \pi/124$, i.e. $J = 6$. Measurements are then transformed using Haar wavelet up to $J = 6$. An explanatory data analysis technique based on scatter plot is adopted to find the significant scales. The scatter plot between observed value and one-step-ahead prediction is plotted in Fig. 6. It can be seen from Fig. 6 that scales $j = 1$ to 3 do not consist of any critical knowledge as compared to scales $j = 4$ to 6, thus the former can be ignored for model estimation. Hence, the models are estimated only at scale $j = 4, 5, 6$ and $J + 1 = 7$ using Akaike's Information Criterion.

4.3 Control Design

In this study, a load-following transient is considered to examine quintessential load variations of ramp and step type. The transient is described as follows:

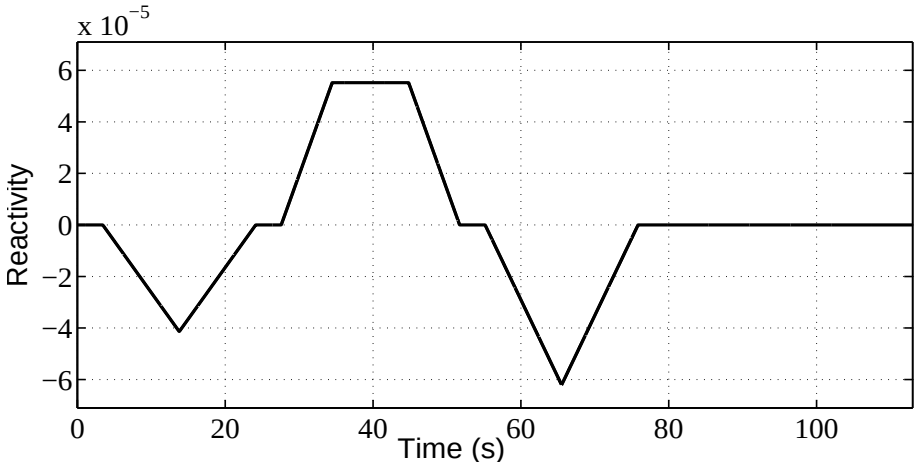

Fig. 3. Assumed reactivity variation (estimation input data).

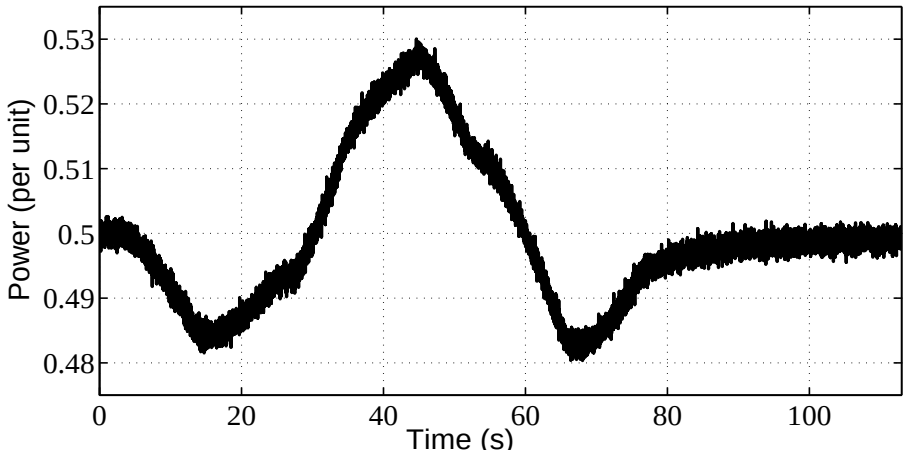

Fig. 4. Reactor power variation corresponding to reactivity variation (estimation output data).

Table 1. Neutronic and thermal-hydraulic parameters

Group, i	1	2	3	4	5	6
$\lambda_i(s^{-1})$	0.0125	0.0308	0.1152	0.3109	1.240	3.3287
β_i	0.000216	0.001416	0.001349	0.00218	0.00095	0.000322
$H_f(^\circ C s^{-1})$	$H_c(s^{-1})$	$\gamma_f(s^{-1})$	$\gamma_c(s^{-1})$	$\alpha_f\left(^\circ C^{-1}\right)$	$\alpha_c\left(^\circ C^{-1}\right)$	$\Lambda(s)$
102.7	0.2401	0.1792	0.0124	-2×10^{-5}	-5×10^{-5}	5×10^{-4}
$\tau_{cold}(s)$	$\tau_{hot}(s)$	$\tau_{sg}(s)$	$D_1(^\circ C s^{-1})$	D_2	D_3	
7.0	5.0	11.3	3.746	0.7005	-0.2995	

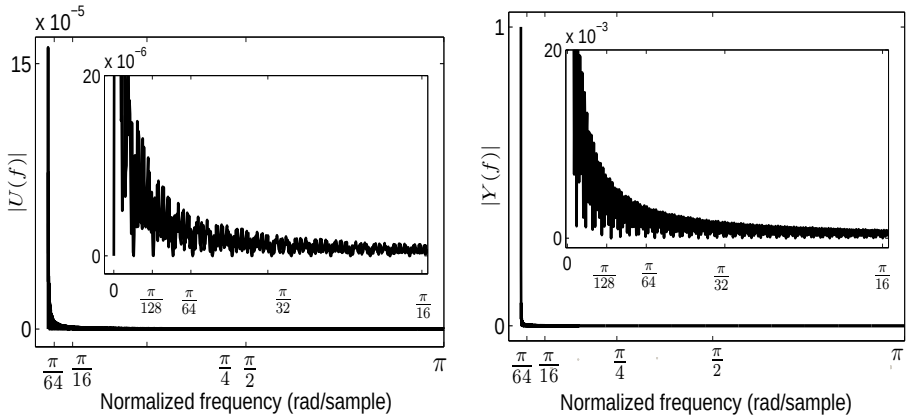

Fig. 5. The discrete-time Fourier transform of the input and output signal.

Initially, the desired power is maintained at 50% full power for 200 s. Then it is varied from 50% to 90% full power in 480 s and held constant at 90% full power for the next 300 s; then it is reduced from 90% to 75% full power in 180 s; held at 75% full power for 300 s; then a 10% step increase is applied at 1460^{th}s; held at 85% full power for 500 s; then a 10% step decrease is applied at 1960^{th}s and held at 75% full power for 540 s [19, 20].

The values of prediction and control horizon for simulation are set to $N_P = 20$ and $N_C = 5$, respectively. Here, constraints on input and output are also taken into account, where the constraints on input determine the insertion/withdrawal limit and the rate of movement of RR whereas the constraint on output limits the maximum power output. For this case study, the following constraints are considered:

$$\begin{aligned} &0.48 \le P \le 0.92, \\ &-5\times10^{-3} \le \rho_{RR} \le 5\times10^{-3}, \\ &-1\times10^{-5} \le \Delta\rho_{RR} \le 1\times10^{-5}. \end{aligned} \tag{26}$$

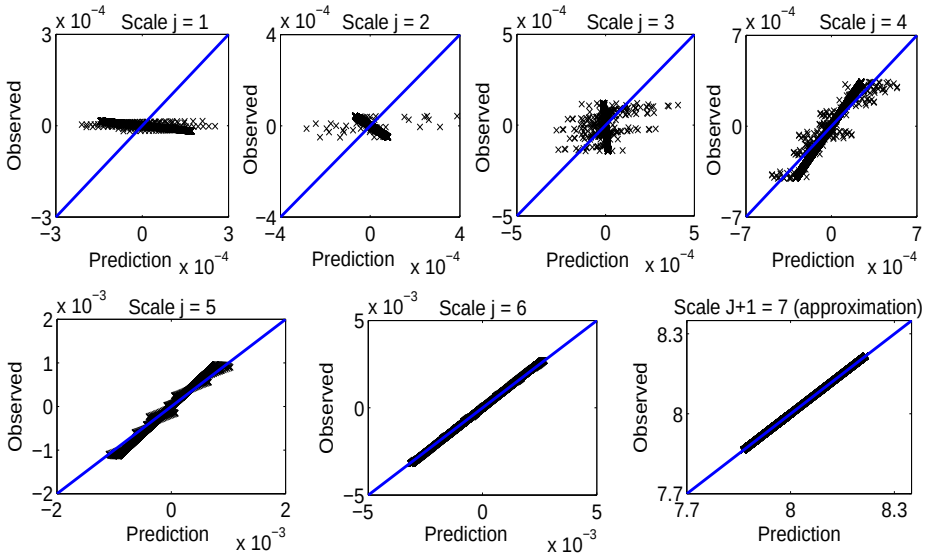

Fig. 6. Scatter plot between observed output and one-step-ahead prediction.

During normal operations of load-following, te set-point variation and the performance of the proposed controller during set-point tracking in the presence of process constraints is shown in Fig. 7. It can be observed that the controller tracks the variation smoothly as envisaged. It is able to handle the 5%/min ramp as well as the 10% step variations in the load. The control signal (ρ_{RR}) and rate of change of controlled signal ($\Delta\rho_{RR}$) variations are also shown in Figs. 8 and 9, respectively.

In addition to the normal mode of operation, the fault-tolerant performance of the proposed controller is also tested in case of an actuator-based fault. Here, a fault due to sudden drop of RR is simulated which introduces negative reactivity in the system. At 980 s, it is considered that due to sudden drop in RR from its nominal position, a negative reactivity of the value 5×10^{-6} is introduced in the system. It can be noted that the controller is unaware of the fault and the input has been reconfigured to adjust for the failure (Figs. 8, 9), with the controller is able to track the set-point (Fig. 7). The proposed controller maintains the process constraints sufficiently in normal operation as well as in the presence of fault and preserves the inherent fault-tolerant capability of an MPC.

5 Conclusions

A predictive control approach using wavelet-based state-space identified model is introduced in the paper. The proposed MPC employs multi-resolution state-space models operating at different time-scales for output prediction. Thus, the resulting control action incorporates contribution from multiple time-scales. The

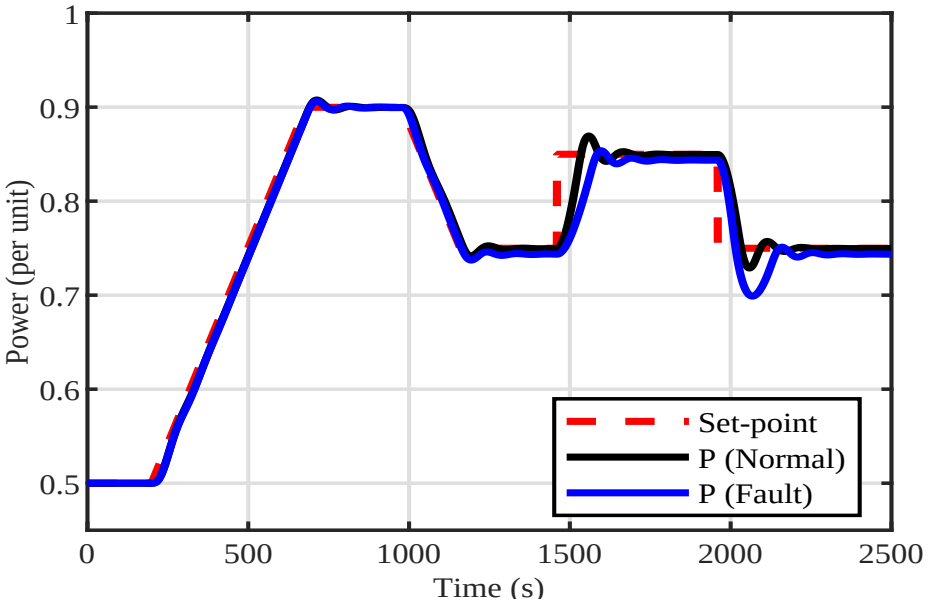

Fig. 7. Load tracking performance of proposed controller during normal and in the presence of a fault.

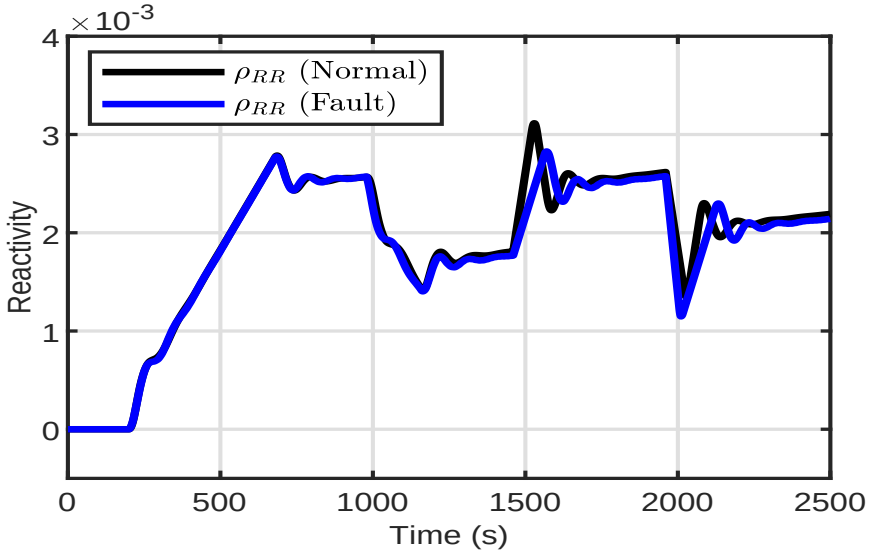

Fig. 8. Variation of control input during normal and in the presence of a fault.

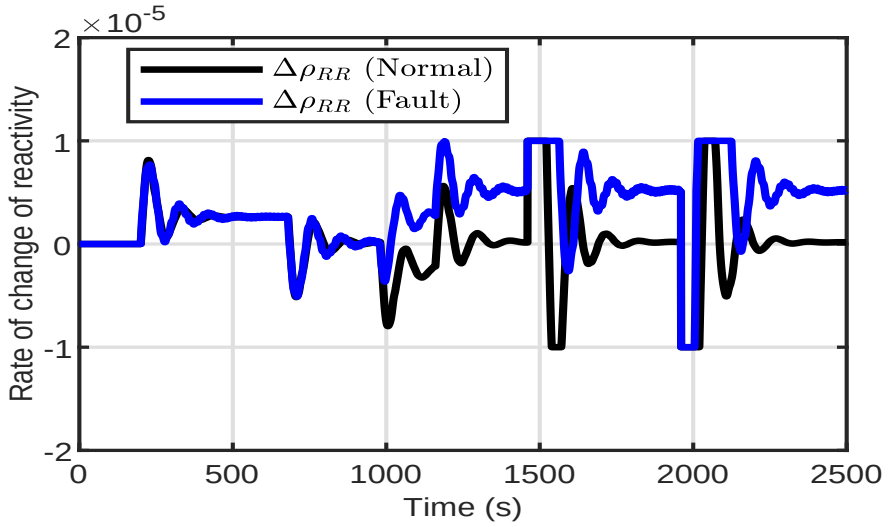

Fig. 9. Variation of rate of change of control input during normal and in the presence of a fault.

controller is applied to the constrained load-following problem of a PWR nuclear reactor. Simulations are performed to study control performances in normal mode of operation as well as in the presence of an actuator-based fault due to sudden drop of RR. The designed control law is found effectively to cope up with step and ramp type transients in the load without violating process constraints and preserves the inherent fault-tolerant capability of an MPC.

References

1. S. J. Qin and T. A. Badgwell, "A survey of industrial model predictive control technology," *Control Engineering Practice*, vol. 11, no. 7, pp. 733–764, 2003.
2. J. M. Maciejowski, "Fault-tolerant aspects of MPC," *IEE Two-Day Workshop on Model Predictive Control: Techniques and Applications - Day 2 (Ref. No. 1999/096), London, UK*, pp. 1/1–1/4, 1999.
3. J. B. Rawlings, "Tutorial overview of model predictive control," *IEEE Control Systems*, vol. 20, no. 3, pp. 38–52, Jun 2000.
4. S. R. Shimjith, A. P. Tiwari, and B. Bandyopadhyay, "A three-timescale approach for design of linear state regulator for spatial control of advanced heavy water reactor," *IEEE Transactions on Nuclear Science*, vol. 58, no. 3, pp. 1264–1276, 2011.
5. A. Elias-Juarez and J. C. Kantor, "On the application of wavelets to model predictive control," in *1992 American Control Conference*, June 1992, pp. 1582–1586.
6. J. H. Lee, Y. Chikkula, Z. Yu, and J. C. Kantor, "Improving computational efficiency of model predictive control algorithm using wavelet transformation," *International Journal of Control*, vol. 61, no. 4, pp. 859–883, 1995.

7. W. Feng, H. Genceli, and M. Nikolaou, "Constrained model predictive control with simultaneous identification using wavelets," *Computers & Chemical Engineering*, vol. 20, pp. S1011–S1016, 1996.
8. M. Basseville, A. Benveniste, K. C. Chou, S. A. Golden, R. Nikoukhah, and A. S. Willsky, "Modeling and estimation of multiresolution stochastic processes," *IEEE Transactions on Information Theory*, vol. 38, no. 2, pp. 766–784, Mar 1992.
9. G. Stephanopoulos, O. Karsligil, and M. Dyer, "Multi-scale aspects in model-predictive control," *Journal of Process Control*, vol. 10, no. 2, pp. 275–282, 2000.
10. ——, "Multiscale theory for linear dynamic processes: Part 2. multiscale model predictive control (MS-MPC)," *Computers & Chemical Engineering*, vol. 32, no. 4, pp. 885–912, 2008.
11. S. Zhang and J. Bentsman, "Wavelet multiresolution model based predictive control for constrained nonlinear systems," in *American Control Conference*, June 2014, pp. 4895–4900.
12. S. Mukhopadhyay and A. P. Tiwari, "A model predictive control strategy based on consistency in wavelet projections," *IFAC Proceedings Volumes*, vol. 47, no. 1, pp. 614–619, 2014.
13. R. Wang, M. J. Tippett, and J. Bao, "Fast wavelet-based model predictive control of differentially flat systems," *Processes*, vol. 3, pp. 161–177, 2015.
14. M. Vetterli and J. Kovacevic, *Wavelets and subband coding*. Prentice Hall , Englewood Cliffs, NJ,, 1993.
15. A. E. Cetin and M. Tofighi, "Projection-based wavelet denoising [lecture notes]," *IEEE Signal Processing Magazine*, vol. 32, no. 5, pp. 120–124, 2015.
16. M. S. Reis, "A multiscale empirical modeling framework for system identification," *Journal of Process Control*, vol. 19, no. 9, pp. 1546–1557, 2009.
17. S. J. Qin, "An overview of subspace identification," *Computers & Chemical Engineering*, vol. 30, no. 10, pp. 1502–1513, 2006.
18. V. Vajpayee, S. Mukhopadhyay, and A. P. Tiwari, "Multiscale subspace identification of nuclear reactor using wavelet basis function," *Annals of Nuclear Energy*, vol. 111, pp. 280–292, 2018.
19. M. G. Na, S. H. Shin, and W. C. Kim, "A model predictive controller for nuclear reactor power," *Journal of Korean Nuclear Society*, vol. 35, no. 5, pp. 399–411, Oct 2003.
20. V. Vajpayee, S. Mukhopadhyay and A. P. Tiwari, "Data-driven subspace predictive control of a nuclear reactor," *IEEE Transactions on Nuclear Science*, vol. 65, no. 2, pp. 666–679, Feb 2018.